Article

Spaced Hybrid TiO₂/Au Nanotube Arrays with Tailored Optical Properties for Surface-Enhanced Raman Scattering

Morteza Afshar, Subrata Ghosh, Luca Mascaretti,* Štěpán Kment, Carlo Spartaco Casari,* and Alberto Naldoni*

Read Online

ACCESS | Metrics & More | Article Recommendations | Supporting Information

ABSTRACT: Controlling the overall geometry of plasmonic materials allows for tailoring their optical response and the effects that can be exploited to enhance the performance of a wide range of devices. This study demonstrates a simple method to control the size and distribution of gold (Au) nanoparticles grown on the surface of spaced titanium dioxide (TiO₂) nanotubes by varying the deposition time of magnetron sputtering. While shorter depositions led to small and well-separated Au nanoparticles, longer depositions promoted the formation of quasi-continuous layers with small interparticle gaps. The optical spectra of Au/TiO₂ nanotubes showed a region of strong absorption (200−550 nm) for all samples and a region of decreasing absorption with an increase of effective Au thickness (550−1100 nm). This behavior led to distinct trends in the Raman signal enhancement of the underlying TiO₂ nanotubes depending on the excitation laser wavelength. Furthermore, the quasi-continuous layers formed at higher effective Au thicknesses promoted an amplification of the signal and an improvement in the detection limit of target molecules in surface-enhanced Raman scattering (SERS) experiments. These findings suggest a simple method for designing efficient devices with tailored light absorption and potential applications in detectors and other optical devices.
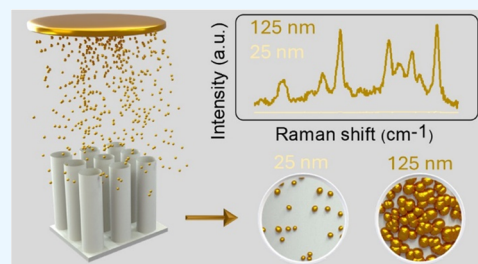
INTRODUCTION

Over the last decades, plasmonic materials have held great importance across various fields due to their unique ability to manipulate and confine light at subwavelength levels and to transform photon energy into heat.[1] The resonance wavelength of these materials and consequently their optical absorption can be adjusted through the manipulation of size, morphology, and overall geometry of their nanostructures as well as the permittivity of the surrounding medium.[2−4] In addition, another intriguing characteristic of plasmonic resonances is their ability to interact with and couple with each other. The interaction between localized surface plasmon resonances (LSPRs) among multiple close-by nanoparticles (NPs) leads to spectral shift and intensification of such resonances, forming the so-called electromagnetic hot-spots.[5,6] The strength of this coupling and the resulting electric field depend crucially on the gap between the NPs and increase exponentially with a decrease in the gap.[6,7] Tailoring these properties is critical to enhance the performance of plasmonic devices in a wide range of applications, such as SERS,[8−10] photothermal therapy,[11−13] solar-thermal conversion,[14,15] and photocatalysis.[16,17]

To optimize the wavelength and intensity of plasmonic resonances, sophisticated template-based procedures such as electron-beam lithography and nanoimprinting offer precise control over the shape, size, and interunit gap or distance of plasmonic nanostructures. However, these methods can be time-consuming and costly, and their resolution hardly allows

the realization of arrays of very small (∼10 nm) close-packed NPs.[18−20] Therefore, it is necessary to develop simple and scalable fabrication methods to realize plasmonic devices with tailored optical properties for a wider range of applications. For example, template-assisted self-assembly of plasmonic metals demonstrated significant potential to achieve ultrahigh optical absorption.[15,21−23] In this strategy, plasmonic NPs are deposited by a physical vapor deposition process into 3D porous structures (such as anodic alumina nanoporous and natural wood), leading to the fabrication of size-distributed NPs with different shapes. Morphological features of the underlying material, therefore, such as the degree of disorder and the pore diameters, have a strong impact on the optical properties of the so-obtained plasmonic nanostructures.[15,24] In this context, utilizing anodic TiO₂ nanotubes (NTs) as a template emerges as a compelling choice, not only due to the ability to precisely control the structure and pore morphology of TiO₂ NT arrays through manipulating anodization parameters,[25,26] but also due to their photocatalytic properties that provide an intriguing structure for a broader range of
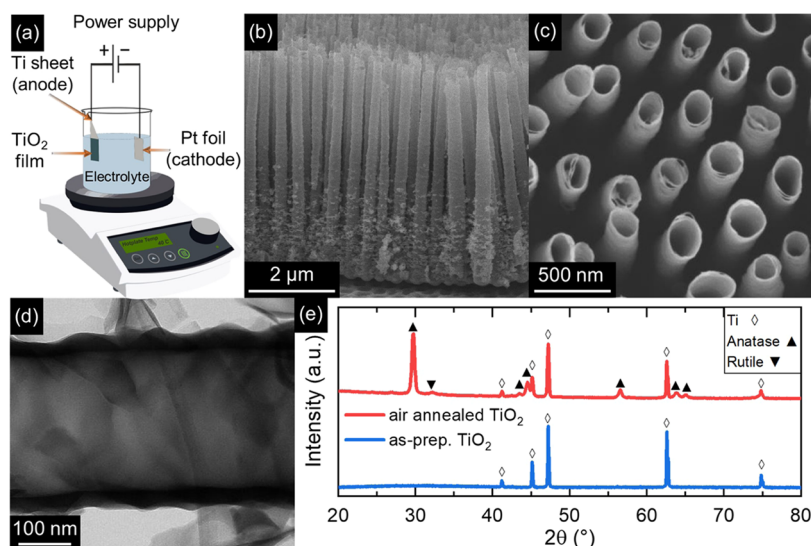
Figure 1. Fabrication and characterization of spaced TiO$_2$ NT arrays. (a) Schematic illustration of the anodization setup employed for the fabrication of TiO$_2$ NTs. (b−d) SEM cross-sectional (b), top-view (c), and TEM (d) images of NT arrays anodized at 60 V for 3 h. (e) X-ray diffraction patterns of as-prepared (blue) and air-annealed (red) TiO$_2$ NT arrays.
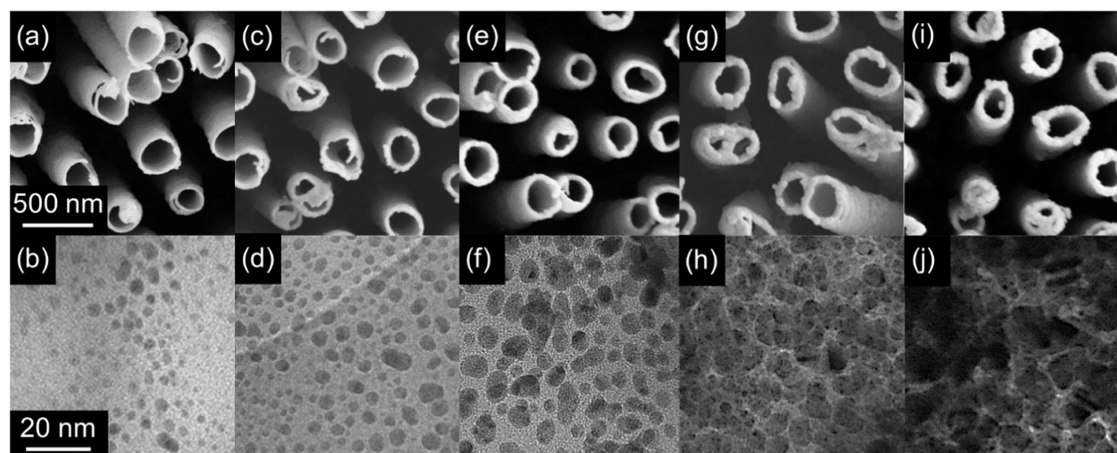

Figure 2. Morphology of TiO$_2$ NTs/Au substrates with different effective thicknesses of Au. (a−j) SEM (first row) and TEM (second row) images of the uppermost portion of NTs deposited with (a, b) 25 nm, (c, d) 50 nm, (e, f) 75 nm, (g, h) 100 nm, and (i, j) 125 nm of Au. Scale bars in (a, b) are applicable to all SEM (first row) and TEM (second row) images, respectively.

applications. For instance, TiO$_2$ NTs can be designed as spaced NTs, which enable the reduction of light reflection, leading to higher light absorption relative to their close-packed counterparts,[26−28] and coating of both the inner and outer surfaces of tubes. While research on template-assisted self-assembly of plasmonic metals has primarily focused on their photothermal applications,[15,23,29] the exploration of their SERS performance remains relatively unexplored.

In this work, we designed a series of spaced TiO$_2$ NTs/Au films with different optical absorption profiles and investigated them as SERS substrates for the detection of organic molecules. Specifically, TiO$_2$ NTs were fabricated through electrochemical anodization, and then, Au NPs were deposited using magnetron sputtering. This approach allowed tailoring the average NP size and interparticle gap distance by controlling the sputter deposition thickness (time), leading to tailored optical properties with two distinct spectral regions of light absorption. Raman spectroscopy experiments with a green laser excitation wavelength revealed a significant decrease in the intensity of underlying TiO$_2$ signals with

increasing Au effective thickness. On the contrary, Raman spectra excited with red laser light demonstrated stronger TiO$_2$ signals for samples with lower absorption and higher thickness of Au. This suggested a higher density of electromagnetic hot-spots on the TiO$_2$ NTs coated with quasi-continuous Au layers. This conclusion was further supported by SERS measurements, which revealed higher activity of these samples for detecting Rhodamine 6G (Rh6G) compared to TiO$_2$/Au samples featuring small and dispersed NPs. Therefore, this work provides a simple and feasible method for fabricating diverse plasmonic nanostructures and tailoring their overall properties for diverse applications.

■ RESULTS AND DISCUSSION

The fabrication of a range of TiO$_2$ NTs/Au substrates featuring tailored absorption profiles and different densities of Au NPs was initiated by the anodization of Ti foil in a two-electrode electrochemical cell for 3 h at a constant applied voltage of 60 V between the electrodes (Figure 1a) to obtain TiO$_2$ NTs as a template. The fabricated NTs exhibited well-
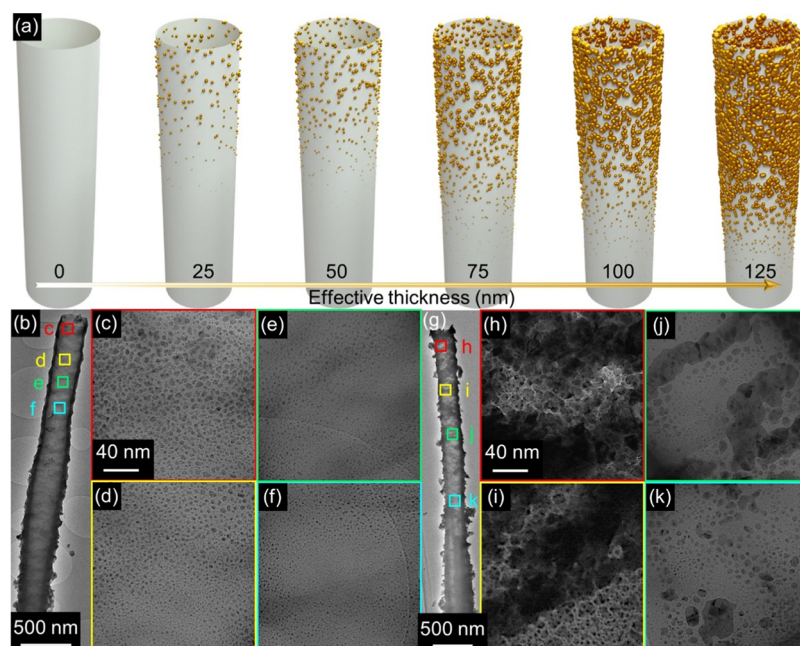
Figure 3. Transformation of the spatial density and morphology of NPs with varying effective thicknesses of deposited Au. (a) The schematic of the nonuniform self-assembly of Au NPs with different Au effective thicknesses on a single NT. (b−k) Low- and high-magnification TEM images of different portions of NT coated with (b−f) 50 nm and (g−k) 125 nm of Au. Scales for panels (d−f) and (i−k) are identical to those shown in panels (c) and (h), respectively.

aligned and distinct structures with a mean length of 5 μm, mean outer and inner diameters of ≈275 and ≈245 nm, respectively, and an average center-to-center distance of 480 nm (Figure 1b−d). Furthermore, the as-prepared NTs exhibited a relatively short-range order. Such features are in agreement with previous works reporting spaced TiO$_2$ NTs.[26,28] X-ray diffraction (XRD) analysis (Figure 1e) of as-prepared TiO$_2$ NTs detected only the characteristic peaks of metallic Ti substrate, implying the amorphous structure of the as-prepared NTs, as typical of anodized TiO$_2$.[25,30] Crystallization into the anatase phase was promoted by air annealing at 450 °C for 2 h. A minor rutile fraction was also revealed by a small diffraction peak at $2\theta \approx 32°$.

TiO$_2$ NTs/Au substrates were achieved by coating the annealed NTs with different amounts of Au NPs by magnetron sputtering. The effective thickness of Au, specifically ∼25, 50, 75, 100, and 125 nm, was varied to control the NPs' distribution and morphology on the surface of the NTs and, further, to decrease the diameter of the NTs themselves, as revealed by SEM and TEM imaging (Figure 2). At the 25 nm thick Au deposition, the average diameter of NTs diminished to ≈240 nm (Figure 2a), and well-dispersed irregularly shaped NPs with a random size distribution, averaging ≈2 nm in diameter, appeared on the uppermost portion of the surface of NTs (Figure 2b). As the thickness of the deposited Au increased to 50 nm (Figure 2c,d), a further decline in the diameter of NTs (≈220 nm) was observed and the small NPs partially coalesced into slightly bigger ones (ranging from 1 to 10 nm and with a mean size of ≈5 nm) with higher density (i.e., smaller interparticle gaps) and random size distribution on the surface. A similar trend was observed by further increasing the effective thickness of the Au deposition to 75 and 100 nm (Figure 2e−2h), where a decrease in the diameter of TiO$_2$ NTs and a coalescence of NPs into bigger particles with higher density and reduced interparticle spacing persisted.

Finally, the highest thickness of Au (125 nm) led to a further decrease of the mean diameter of NTs (≈160 nm) and to the formation of a quasi-continuous layer of Au (NPs spaced by a distance of ≈1 nm; Figure 2i,2j).

Au coating on TiO$_2$ NTs by sputtering led to a gradient of NP spatial density, size distributions, and morphology along the tube length (Figure 3). Figure 3a provides a schematic representation of such a deposition of Au NPs on both the interior and exterior surfaces of NTs coated with different thicknesses. NTs coated with lower thicknesses of Au (25−75 nm) exhibited a gradual decrease in the spatial density and mean diameter of the Au NPs by moving from the upper to lower portion of the NTs. For example, in the case of NTs coated with 50 nm of Au (Figure 3b), the mean diameter of Au NPs decreased from ≈5 nm (Figure 3c) to ≈1 nm, moving from the tube mouth region to the middle one (Figure 3d−3f). A similar effect was observed in NTs with higher thickness of Au (100 and 125 nm). For instance, in the case of NTs coated with 125 nm of Au (Figure 3g), a quasi-continuous Au layer appeared in correspondence with the tube mouth (Figure 3h), while the areas closer to the lower portions of the tube exhibited a progressively lower density of Au coating and the appearance of well-spaced isolated NPs (Figure 3i−3k). Therefore, not only the effective Au thickness but also the distance from the tube mouth influenced the morphology of Au NPs grown on the NT surface. This is expected for a highly directional process such as magnetron sputtering, where the deposited species mostly travel in straight lines from the target to the substrate.[31] Therefore, the upper portions of the NTs could act as physical barriers, thus hampering the arrival of Au to the tube's lower portions. Nevertheless, despite the length of the NTs (5 μm; Figure 1), the tube-to-tube spacing allowed Au coating even in the lower portions of the tubes.[32,33] As a consequence, hierarchical functionalization of nearly all of the
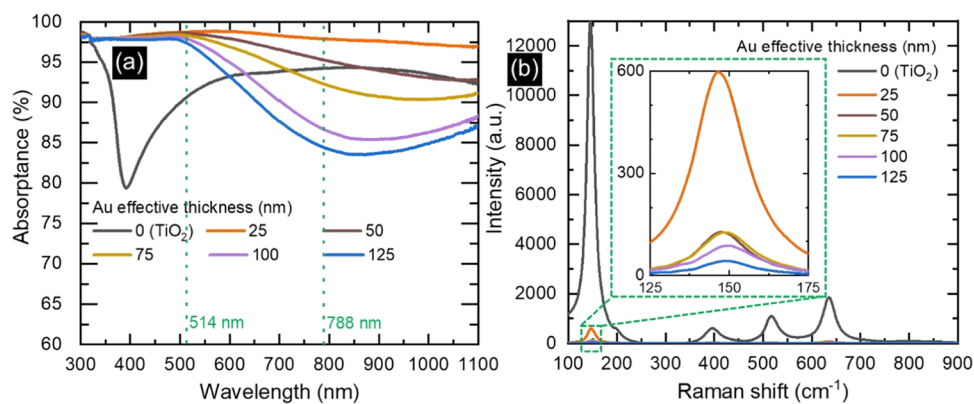
Figure 4. Impact of different effective Au thicknesses on the optical properties and Raman spectra of TiO_2/Au NTs. (a) Optical absorption and (b) Raman spectra under a 514 nm laser light excitation of bare and coated TiO_2 NTs. The inset in panel (b) presents an enlarged view of the main anatase Raman peak.
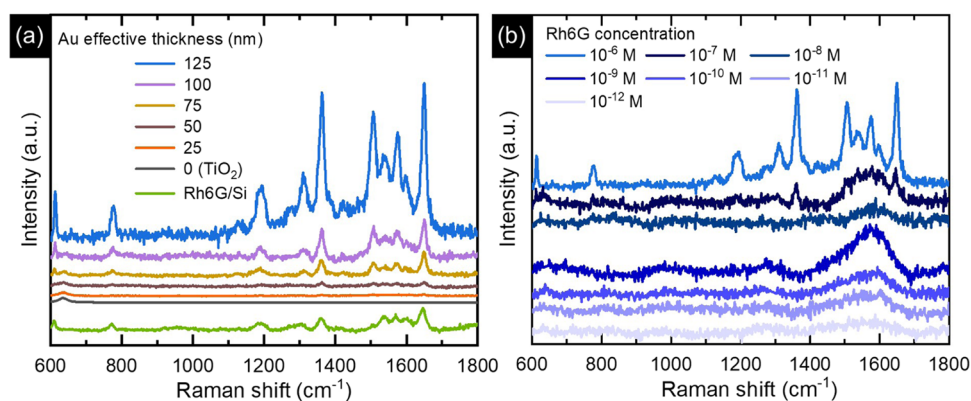

Figure 5. SERS application of TiO_2 NTs/Au substrates. SERS spectra of (a) 10^{-6} M Rh6G deposited on TiO_2 NTs with different effective thicknesses of Au and Rh6G powder on Si (b) Rh6G at varied concentrations deposited on the TiO_2 NTs with 125 nm thick Au. SERS spectra for TiO_2/Au NTs are normalized to the intensity of the E_g mode of the TiO_2 peak at 144 cm^{-1} to allow direct comparison of relative peak intensities.

TiO_2 surface with Au was achieved, which was desired in light of the SERS application (see below).

The varying amounts of sputtered Au and consequently different densities and morphological alterations of the hierarchical structure in each sample significantly impacted the optical properties of NTs (Figure 4a). Specifically, the annealed TiO_2 sample without Au demonstrated a blue color (Figure S1a) with a distinct absorption edge at ~390 nm and a broad-band absorption peak in the visible region. These spectral features were attributed to the band-gap energy of anatase TiO_2 (3.24 eV) and the specific morphology of NTs.[28,34] In contrast, the sample with 25 nm thick Au displayed a black color (Figure S1b) and a broad-band absorption surpassing 97% in the wavelength region of 300–1100 nm. Such a high and broad-band absorption may originate from the synergistic interplay of two key elements. The high fraction of air trapped in the trough area inside and between NT arrays and the gradual increase of the thickness of NTs (Figure 3b) from the top ($\approx$25 nm) to the bottom ($\approx$80 nm) could minimize the optical index or impedance difference at the interface between air and substrate, resulting in an antireflection effect.[15,35,36] On the other hand, the randomly arranged Au NPs with different sizes on the surface of NTs with an uneven tube-to-tube distance may lead to the superposition of multiple LSPR modes, in turn leading to broad-band absorption spectra.[15,29,37,38] By increasing the effective thickness of Au further, the appearance of samples

changed from black to brown (Figure S1) and, indeed, the optical absorption in the wavelength region >550 nm monotonically decreased, showing a broad minimum at ~850 nm (Figure 4a). Conversely, no significant change in absorption spectra was found at wavelengths <550 nm. Such a trend can be ascribed to the gradual coalescence of well-dispersed NPs with different shapes into slightly bigger NPs with lower interparticle distance and, ultimately, into a semicontinuous film (Figure 2), therefore resembling a reflecting metallic Au film. These results suggest the potential of such hybrid TiO_2/Au structures with tailored optical properties for different desired applications. For example, TiO_2 NTs coated with smaller Au NPs and displaying higher optical absorption may be well-suited for photothermal and catalytic applications,[15,39-41] while those featuring partially coalesced Au NPs or quasi-continuous coatings could be ideal for SERS applications.[5,8]

Since the TiO_2/Au NTs exhibited two distinct regimes of constant and monotonically decreasing optical absorption with respect to the effective Au thickness, two different laser lines (i.e., 514.5 and 788 nm, marked by dotted lines in Figure 4a) were employed to perform Raman spectroscopy experiments. Raman spectra exhibited the characteristic peaks of anatase TiO_2 at 144, 197, 399, 516, and 639 cm^{-1}, which, respectively, correspond to the E_g, E_g, B_{1g}, $A_{1g}+B_{1g}$, and E_g vibrational modes (Figures 4b and S2).[42,43] Specifically, Raman spectra acquired under a 514.5 nm laser excitation on the TiO_2 NTs with 25 nm

of Au exhibited a significant decrease in intensity compared to that of uncoated TiO$_2$ NTs (see the main anatase peak at 144 cm^{-1}; inset in Figure 4b). This effect could be attributed to the significant absorption of light with Au NPs. Further increasing the effective thickness of Au, with a nearly constant and high optical absorption, led to further limiting the penetration and interaction of light with the underlying TiO$_2$, resulting in lower Raman intensities. In contrast, Raman spectra acquired under a 788 nm laser excitation revealed the opposite trend; i.e., the intensity increased by increasing the Au effective thickness (Figure S2). Particularly, the NTs with a 125 nm thick Au overlayer exhibited the highest Raman intensity, even more than pure TiO$_2$ NTs. This observation is in line with previous studies[44−46] and can be explained by a SERS effect on the anatase peaks. In this regime, the lower absorption by the Au quasi-continuous films may allow sufficient light penetration to the underlying TiO$_2$ and intensification of Raman scattering by electromagnetic hot-spots in Au. On the other hand, the same did not occur under a 514.5 nm excitation, which could suggest a nearly complete light absorption by the Au overlayer due to its high absorption at this wavelength.

The results of Raman spectroscopy on TiO$_2$/Au NPs suggest that a 514.5 nm laser excitation may be suitable for confining the optical absorption in the Au NP layer and consequently generating strong plasmonic resonances to probe SERS spectra of molecules adsorbed to the Au surface. For this purpose, the SERS activity of these samples was evaluated for the detection of Rh6G molecules (Figure 5). Figure 5a shows the Raman spectra of Rh6G in its powder form deposited on a Si substrate and its 10^{-6} M solution drop-coated on TiO$_2$ and TiO$_2$/Au NTs. The Raman spectrum of bare Rh6G powder consists of peaks at around 611 (C−C−C ring in-plane bending vibration), 775 (C−H out-of-plane bending vibration), and 1306, 1360, 1541, 1573, 1600, and 1648 cm^{-1} (aromatic stretching vibrations). For the sake of comparison, we coated 10^{-6} M Rh6G on a Si substrate and Ti foil (not shown), and no apparent peaks of Rh6G were observed on either. Moreover, no Rh6G peaks were observed from the bare TiO$_2$ NTs and TiO$_2$ NTs with 25 nm of Au. When the Au effective thickness increased from 50 to 125 nm on the TiO$_2$ NTs, the Raman signal was found to be enhanced. Specifically, a very weak Raman intensity was observed from 50 nm Au-coated TiO$_2$ NTs, and the most intense signals were observed from 125 nm Au-coated ones. In order to quantify the enhancement effect, we estimated the intensity ratio, considering the maximum heights of the most intense Rh6G peak (1648 cm^{-1}) and TiO$_2$ anatase peak (144 cm^{-1}). The intensity ratio I_{1648}/I_{144} of TiO$_2$/Au NTs was found to be 0.21, 0.93, 1.64, and 6.45 for the NTs with 50, 75, 100, and 125 nm effective thicknesses of Au, respectively. Such a trend emphasizes the paramount importance of bigger and partially coalesced particles leading to electric field hot-spots between the interparticle gaps, which in turn may explain the higher SERS performance. To support this conclusion and elucidate the influence of NTs in enhancing Raman intensity, a 125 nm Au film was deposited onto Ti foil, which led to the growth of a continuous metal layer (Figure S3a). Afterward, the SERS activity of this sample was compared to that observed on the TiO$_2$ NTs with 125 nm thick Au (Figure S3b). The SERS spectrum obtained from Ti/Au exhibited only a few peaks at 1360, 1541, 1573, and 1648 cm^{-1}, while other vibrations were hardly detected. Moreover, the intensity of the observed SERS peaks with the Ti/Au sample was comparatively lower than

that measured in the presence of spaced TiO$_2$ NTs as a platform for the growth of Au NPs. The intensity ratio of the 1648 cm^{-1} peak for TiO$_2$/Au NTs to Ti/Au (i.e., I_{1648}(TiO$_2$/Au)/I_{1648}(Ti/Au)) was found to be around 1.65. These observations suggest that the morphology of the Au layer (i.e., partially coalesced NPs vs continuous film) can have a significant impact on not only the entire spectral fingerprint but also the intensity of SERS peaks. Further measurements of the SERS effect of Rh6G molecules with lower concentrations (10^{-7}−10^{-12} M) indicated that the 125 nm Au-coated NTs could be effective in determining the lower amount of these molecules (Figure 5b). At this point, it is worth pointing out that although the presented spaced TiO$_2$/Au structures represented a scalable option for the realization of SERS substrates and their flexible plasmonic tunability may be further explored in other kinds of detection or solar energy conversion devices, it did not reach the detection limit of other substrates reported in the literature.[47,48] Nevertheless, further optimization could lead to enhancing the overall performance. For instance, manipulating anodization parameters allows us to achieve lower space between and inside the NTs, making the Au NPs closer to others leading to a higher concentration of the hot-spots and subsequently higher SERS enhancement, or air annealing after Au deposition to modify the shape and size distribution of the Au NPs.[49,50]

CONCLUSIONS

In summary, this study demonstrated a promising strategy for tailoring the optical properties of plasmonic Au NPs grown on anodic TiO$_2$ NTs by simply controlling the sputter deposition effective thickness. A controlled transition from small and well-separated Au NPs to quasi-continuous layers on the TiO$_2$ surface was achieved, which in turn affected the optical properties of the composite TiO$_2$/Au NTs. The sample with the lowest effective thickness of Au exhibited broad-band light absorption, which was attributed to a superposition of multiple LSPRs. On the other hand, the optical absorption monotonically decreased at wavelengths longer than 550 nm by increasing the effective Au thickness. Raman spectra revealed the role of morphology and optical absorption in detecting the underlying TiO$_2$. A significantly lower intensity of anatase TiO$_2$ signals in TiO$_2$/Au compared to that of uncoated TiO$_2$ NTs was found using a green (514.5 nm) excitation laser wavelength, thus corresponding to the high absorption region (514 nm). An opposite trend was observed under a red (788 nm) laser excitation. Furthermore, the TiO$_2$ NTs with 125 nm thick Au showed the highest SERS enhancement for the Rh6G molecule, which was explained by a higher density of electromagnetic hot-spots within the narrow interparticle gaps. These findings highlight a straightforward strategy to systematically tune the optical properties of plasmonic NPs grown on a nanostructured substrate, which is relevant not only for SERS devices but also for solar energy conversion devices.

METHODS

Sample Preparation. The fabrication of spaced TiO$_2$ NTs involved the anodization of a titanium (Ti) foil in a two-electrode electrochemical cell, using the Ti foil (0.25 mm thick) as the working electrode and a Pt sheet as the counter electrode. Before anodization, the process was initiated through a three-step ultrasonic cleaning of a commercial Ti

foil in acetone, ethanol, and distilled water for about 15 min, followed by drying under a nitrogen stream to eliminate surface impurities. Subsequently, anodization of the foil was carried out in diethylene glycol (DEG) electrolyte containing 0.5 wt % NH_4F_2 and 3.6 wt % H_2O at a constant voltage of 60 V for 3 h at 40 °C. Following anodization, the obtained TiO_2 NTs were thoroughly washed with ethanol and water followed by drying under a nitrogen flow to ensure the removal of the residual electrolyte. Subsequently, crystalline TiO_2 was achieved through annealing of the sample for 2 h in an air atmosphere at 450 °C by heating and cooling ramp of 2 °C/min. Finally, to obtain a TiO_2 NTs\Au substrate, a Quorum sputtering machine (Q150T ES plus) was employed to decorate the NTs with various effective thicknesses of 25, 50, 75, 100, and 125 nm Au. The effective thickness was determined by sputtering the Au layer onto a Si substrate for a distinct time and then measuring the thickness of the deposited layer using cross-sectional SEM.

Characterization. Scanning electron microscopy (SEM, Hitachi FE-SEM 4800) and transmission electron microscopy (TEM JEOL 2010) were employed to investigate the morphology of the prepared samples. An X-ray diffractometer (XRD, PANalytical, Almelo, The Netherlands) with Co–Kα radiation (λ = 0.179 nm) operated in the Bragg–Brentano geometry was used to determine the crystal structure. The optical property measurements were carried out using a Specord-250 Plus spectrometer attached to an integrating sphere (Analytik Jena GmbH, Germany) for reflectance (R) measurement in the 300–1100 nm range. The absorptance (A) was then calculated by A = 1-R, and the opaque nature of Ti substrates across the entire investigated spectral range permits the exclusion of the transmittance (T). Raman measurements were recorded employing a DXR Raman spectrometer (Thermo Scientific) using lasers operating at 514.5 and 788 nm at a power of 0.1 mW to minimize any potential sample damage during measurement. To ensure the precision and accuracy of the obtained data, five spots on the surface of each sample were measured, and the averaged outcome was presented. To evaluate the SERS activity of the samples, an InVia Raman spectrometer (Renishaw) equipped with a 514.5 nm laser source with 1800 gratings and a 20× objective lens was used. For each measurement, a 10 μL aqueous solution of Rh6G of desired concentrations (10^{-6}–10^{-12} M) was drop-casted onto the samples and dried under a table lamp for 1 h before SERS measurements. Then, SERS spectra were collected at a laser power of 0.4 mW with an integration time of 10 s and 50 accumulations per spectrum.

■ ASSOCIATED CONTENT

ⓈI Supporting Information

The Supporting Information is available free of charge at https://pubs.acs.org/doi/10.1021/acsomega.4c05485.

> Optical photographs of bare and coated TiO_2 NTs; Raman spectra of anatase TiO_2 for bare and coated NTs under a 788 nm laser light excitation; and SEM image of the Ti foil coated with 125 nm of Au and corresponding SERS spectra of 10^{-6} M Rh6G compared with that of TiO_2 NTs with 125 nm thick Au (PDF)

■ AUTHOR INFORMATION

Corresponding Authors

Luca Mascaretti − *Czech Advanced Technology and Research Institute (CATRIN), Regional Centre of Advanced Technologies and Materials Department, Palacký University Olomouc, Olomouc 78371, Czech Republic; Department of Laser Physics and Photonics, Faculty of Nuclear Sciences and Physical Engineering, Czech Technical University in Prague, 11519 Prague, Czech Republic;* ⓞ orcid.org/0000-0001-8997-7018; Email: luca.mascaretti@upol.cz

Carlo Spartaco Casari − *Micro and Nanostructured Materials Laboratory (NanoLab), Department of Energy, Politecnico di Milano, Milano 20133, Italy;* ⓞ orcid.org/0000-0001-9144-6822; Email: carlo.casari@polimi.it

Alberto Naldoni − *Czech Advanced Technology and Research Institute (CATRIN), Regional Centre of Advanced Technologies and Materials Department, Palacký University Olomouc, Olomouc 78371, Czech Republic; Department of Chemistry and NIS Centre, University of Turin, Turin 10125, Italy;* ⓞ orcid.org/0000-0001-5932-2125; Email: alberto.naldoni@unito.it

Authors

Morteza Afshar − *Czech Advanced Technology and Research Institute (CATRIN), Regional Centre of Advanced Technologies and Materials Department, Palacký University Olomouc, Olomouc 78371, Czech Republic; Department of Physical Chemistry, Faculty of Science, Palacký University, 779 00 Olomouc, Czech Republic*

Subrata Ghosh − *Micro and Nanostructured Materials Laboratory (NanoLab), Department of Energy, Politecnico di Milano, Milano 20133, Italy;* ⓞ orcid.org/0000-0002-5189-7853

Štěpán Kment − *Czech Advanced Technology and Research Institute (CATRIN), Regional Centre of Advanced Technologies and Materials Department, Palacký University Olomouc, Olomouc 78371, Czech Republic; CEET, Nanotechnology Centre, VŠB-Technical University of Ostrava, Ostrava-Poruba 708 00, Czech Republic;* ⓞ orcid.org/0000-0002-6381-5093

Complete contact information is available at:
https://pubs.acs.org/10.1021/acsomega.4c05485

■ REFERENCES

(1) Gwo, S. *Plasmonic Materials and Metastructures: Fundamentals, Current Status, and Perspectives*; Elsevier: S.l., 2024.

(2) Yu, H.; Peng, Y.; Yang, Y.; Li, Z.-Y. Plasmon-Enhanced Light−Matter Interactions and Applications. *Npj Comput. Mater.* **2019**, *5* (1), 45.

(3) Hartland, G. V. Optical Studies of Dynamics in Noble Metal Nanostructures. *Chem. Rev.* **2011**, *111* (6), 3858−3887.

(4) *UV−VIS and Photoluminescence Spectroscopy for Nanomaterials Characterization*; Kumar, C., Ed.; Springer Berlin Heidelberg: Berlin, Heidelberg, 2013.

(5) Ding, S.-Y.; Yi, J.; Li, J.-F.; Ren, B.; Wu, D.-Y.; Panneerselvam, R.; Tian, Z.-Q. Nanostructure-Based Plasmon-Enhanced Raman Spectroscopy for Surface Analysis of Materials. *Nat. Rev. Mater.* **2016**, *1* (6), No. 16021.

(6) Etchegoin, P. G.; Le Ru, E. C. A Perspective on Single Molecule SERS: Current Status and Future Challenges. *Phys. Chem. Chem. Phys.* **2008**, *10* (40), 6079.

(7) Lee, D.; Yoon, S. Effect of Nanogap Curvature on SERS: A Finite-Difference Time-Domain Study. *J. Phys. Chem. C* **2016**, *120* (37), 20642−20650.

(8) Langer, J.; Jimenez De Aberasturi, D.; Aizpurua, J.; Alvarez-Puebla, R. A.; Auguié, B.; Baumberg, J. J.; Bazan, G. C.; Bell, S. E. J.; Boisen, A.; Brolo, A. G.; Choo, J.; Cialla-May, D.; Deckert, V.; Fabris, L.; Faulds, K.; García De Abajo, F. J.; Goodacre, R.; Graham, D.; Haes, A. J.; Haynes, C. L.; Huck, C.; Itoh, T.; Käll, M.; Kneipp, J.; Kotov, N. A.; Kuang, H.; Le Ru, E. C.; Lee, H. K.; Li, J.-F.; Ling, X. Y.; Maier, S. A.; Mayerhöfer, T.; Moskovits, M.; Murakoshi, K.; Nam, J.-M.; Nie, S.; Ozaki, Y.; Pastoriza-Santos, I.; Perez-Juste, J.; Popp, J.; Pucci, A.; Reich, S.; Ren, B.; Schatz, G. C.; Shegai, T.; Schlücker, S.; Tay, L.-L.; Thomas, K. G.; Tian, Z.-Q.; Van Duyne, R. P.; Vo-Dinh, T.; Wang, Y.; Willets, K. A.; Xu, C.; Xu, H.; Xu, Y.; Yamamoto, Y. S.; Zhao, B.; Liz-Marzán, L. M. Present and Future of Surface-Enhanced Raman Scattering. *ACS Nano* **2020**, *14* (1), 28−117.

(9) Kim, J.; Lee, C.; Lee, Y.; Lee, J.; Park, S.; Park, S.; Nam, J. Synthesis, Assembly, Optical Properties, and Sensing Applications of Plasmonic Gap Nanostructures. *Adv. Mater.* **2021**, *33* (46), No. 2006966.

(10) Li, C.; Man, B.; Zhang, C.; Yu, J.; Liu, G.; Tian, M.; Li, Z.; Zhao, X.; Wang, Z.; Cui, W.; Wang, T.; Wang, J.; Lin, X.; Xu, S. Strong Plasmon Resonance Coupling in Micro-Extraction SERS Membrane for in Situ Detection of Molecular Aqueous Solutions. *Sens. Actuators B Chem.* **2024**, *398*, No. 134767.

(11) Tabish, T. A.; Dey, P.; Mosca, S.; Salimi, M.; Palombo, F.; Matousek, P.; Stone, N. Smart Gold Nanostructures for Light Mediated Cancer Theranostics: Combining Optical Diagnostics with Photothermal Therapy. *Adv. Sci.* **2020**, *7* (15), No. 1903441.

(12) Chen, J.; Gong, M.; Fan, Y.; Feng, J.; Han, L.; Xin, H. L.; Cao, M.; Zhang, Q.; Zhang, D.; Lei, D.; Yin, Y. Collective Plasmon Coupling in Gold Nanoparticle Clusters for Highly Efficient Photothermal Therapy. *ACS Nano* **2022**, *16* (1), 910−920.

(13) Hu, Y.; Liu, X.; Cai, Z.; Zhang, H.; Gao, H.; He, W.; Wu, P.; Cai, C.; Zhu, J.-J.; Yan, Z. Enhancing the Plasmon Resonance Absorption of Multibranched Gold Nanoparticles in the Near-Infrared Region for Photothermal Cancer Therapy: Theoretical

(14) Gao, M.; Zhu, L.; Peh, C. K.; Ho, G. W. Solar Absorber Material and System Designs for Photothermal Water Vaporization towards Clean Water and Energy Production. *Energy Environ. Sci.* **2019**, *12* (3), 841−864.

(15) Zhou, L.; Tan, Y.; Ji, D.; Zhu, B.; Zhang, P.; Xu, J.; Gan, Q.; Yu, Z.; Zhu, J. Self-Assembly of Highly Efficient, Broadband Plasmonic Absorbers for Solar Steam Generation. *Sci. Adv.* **2016**, *2* (4), No. e1501227.

(16) Yu, Y.; Xie, Y.; Zhang, P.; Zhang, W.; Wang, W.; Zhang, S.; Ou, Q.; Li, W. Hot Spots Engineering by Dielectric Support for Enhanced Photocatalytic Redox Reactions. *Nano Res.* **2023**, *16* (1), 239−247.

(17) Liu, D.; Xue, C. Plasmonic Coupling Architectures for Enhanced Photocatalysis. *Adv. Mater.* **2021**, *33* (46), No. 2005738.

(18) Duan, H.; Hu, H.; Kumar, K.; Shen, Z.; Yang, J. K. W. Direct and Reliable Patterning of Plasmonic Nanostructures with Sub-10-Nm Gaps. *ACS Nano* **2011**, *5* (9), 7593−7600.

(19) Chen, Y.; Li, H.; Chen, J.; Li, D.; Zhang, M.; Yu, G.; Jiang, L.; Zong, Y.; Dong, B.; Zeng, Z.; Wang, Y.; Chi, L. Self-Generating Nanogaps for Highly Effective Surface-Enhanced Raman Spectroscopy. *Nano Res.* **2022**, *15* (4), 3496−3503.

(20) Ding, T.; Herrmann, L. O.; De Nijs, B.; Benz, F.; Baumberg, J. J. Self-Aligned Colloidal Lithography for Controllable and Tuneable Plasmonic Nanogaps. *Small* **2015**, *11* (18), 2139−2143.

(21) Wang, Z.; Horseman, T.; Straub, A. P.; Yip, N. Y.; Li, D.; Elimelech, M.; Lin, S. Pathways and Challenges for Efficient Solar-Thermal Desalination. *Sci. Adv.* **2019**, *5* (7), No. eaax0763.

(22) Zhao, F.; Guo, Y.; Zhou, X.; Shi, W.; Yu, G. Materials for Solar-Powered Water Evaporation. *Nat. Rev. Mater.* **2020**, *5* (5), 388−401.

(23) Zhu, M.; Li, Y.; Chen, F.; Zhu, X.; Dai, J.; Li, Y.; Yang, Z.; Yan, X.; Song, J.; Wang, Y.; Hitz, E.; Luo, W.; Lu, M.; Yang, B.; Hu, L. Plasmonic Wood for High-Efficiency Solar Steam Generation. *Adv. Energy Mater.* **2018**, *8* (4), No. 1701028.

(24) Dzhagan, V.; Mazur, N.; Kapush, O.; Skoryk, M.; Pirko, Y.; Yemets, A.; Dzhahan, V.; Shepeliavyi, P.; Valakh, M.; Yukhymchuk, V. Self-Organized SERS Substrates with Efficient Analyte Enrichment in the Hot Spots. *ACS Omega* **2024**, *9* (4), 4819−4830.

(25) Riboni, F.; Nguyen, N. T.; So, S.; Schmuki, P. Aligned Metal Oxide Nanotube Arrays: Key-Aspects of Anodic TiO₂ Nanotube Formation and Properties. *Nanoscale Horiz.* **2016**, *1* (6), 445−466.

(26) Ozkan, S.; Mazare, A.; Schmuki, P. Critical Parameters and Factors in the Formation of Spaced TiO2 Nanotubes by Self-Organizing Anodization. *Electrochim. Acta* **2018**, *268*, 435−447.

(27) Ozkan, S.; Nguyen, N. T.; Mazare, A.; Schmuki, P. Optimized Spacing between TiO₂ Nanotubes for Enhanced Light Harvesting and Charge Transfer. *ChemElectroChem.* **2018**, *5* (21), 3183−3190.

(28) Wawrzyniak, J.; Grochowska, K.; Karczewski, J.; Kupracz, P.; Ryl, J.; Dołęga, A.; Siuzdak, K. The Geometry of Free-Standing Titania Nanotubes as a Critical Factor Controlling Their Optical and Photoelectrochemical Performance. *Surf. Coat. Technol.* **2020**, *389*, No. 125628.

(29) Zhou, L.; Tan, Y.; Wang, J.; Xu, W.; Yuan, Y.; Cai, W.; Zhu, S.; Zhu, J. 3D Self-Assembly of Aluminium Nanoparticles for Plasmon-Enhanced Solar Desalination. *Nat. Photonics* **2016**, *10* (6), 393−398.

(30) Lee, K.; Mazare, A.; Schmuki, P. One-Dimensional Titanium Dioxide Nanomaterials: Nanotubes. *Chem. Rev.* **2014**, *114* (19), 9385−9454.

(31) Gudmundsson, J. T. Physics and Technology of Magnetron Sputtering Discharges. *Plasma Sources Sci. Technol.* **2020**, *29* (11), No. 113001.

(32) Ozkan, S.; Nguyen, N. T.; Hwang, I.; Mazare, A.; Schmuki, P. Highly Conducting Spaced TiO₂ Nanotubes Enable Defined Conformal Coating with Nanocrystalline Nb₂O₅ and High Performance Supercapacitor Applications. *Small* **2017**, *13* (14), No. 1603821.

(33) Ozkan, S.; Yoo, J.; Nguyen, N. T.; Mohajernia, S.; Zazpe, R.; Prikryl, J.; Macak, J. M.; Schmuki, P. Spaced TiO₂ Nanotubes Enable

Optimized Pt Atomic Layer Deposition for Efficient Photocatalytic H$_2$ Generation. *ChemistryOpen* **2018**, 7 (10), 797−802.

(34) Tesler, A. B.; Altomare, M.; Schmuki, P. Morphology and Optical Properties of Highly Ordered TiO$_2$ Nanotubes Grown in NH$_4$F/o-H$_3$PO$_4$ Electrolytes in View of Light-Harvesting and Catalytic Applications. *ACS Appl. Nano Mater.* **2020**, 3 (11), 10646−10658.

(35) Xi, J.-Q.; Schubert, M. F.; Kim, J. K.; Schubert, E. F.; Chen, M.; Lin, S.-Y.; Liu, W.; Smart, J. A. Optical Thin-Film Materials with Low Refractive Index for Broadband Elimination of Fresnel Reflection. *Nat. Photonics* **2007**, 1 (3), 176−179.

(36) Raut, H. K.; Ganesh, V. A.; Nair, A. S.; Ramakrishna, S. Anti-Reflective Coatings: A Critical, in-Depth Review. *Energy Environ. Sci.* **2011**, 4 (10), 3779.

(37) Zhang, F.; Tang, F.; Xu, X.; Adam, P.-M.; Martin, J.; Plain, J. Influence of Order-to-Disorder Transitions on the Optical Properties of the Aluminum Plasmonic Metasurface. *Nanoscale* **2020**, 12 (45), 23173−23182.

(38) Palani, S.; Kenison, J. P.; Sabuncu, S.; Huang, T.; Civitci, F.; Esener, S.; Nan, X. Multispectral Localized Surface Plasmon Resonance (msLSPR) Reveals and Overcomes Spectral and Sensing Heterogeneities of Single Gold Nanoparticles. *ACS Nano* **2023**, 17 (3), 2266−2278.

(39) Henrotte, O.; Santiago, E. Y.; Movsesyan, A.; Mascaretti, L.; Afshar, M.; Minguzzi, A.; Vertova, A.; Wang, Z. M.; Zboril, R.; Kment, S.; Govorov, A. O.; Naldoni, A. Local Photochemical Nanoscopy of Hot-Carrier-Driven Catalytic Reactions Using Plasmonic Nano-systems. *ACS Nano* **2023**, 17 (12), 11427−11438.

(40) Reineck, P.; Brick, D.; Mulvaney, P.; Bach, U. Plasmonic Hot Electron Solar Cells: The Effect of Nanoparticle Size on Quantum Efficiency. *J. Phys. Chem. Lett.* **2016**, 7 (20), 4137−4141.

(41) Kim, H. J.; Lee, S. H.; Upadhye, A. A.; Ro, I.; Tejedor-Tejedor, M. I.; Anderson, M. A.; Kim, W. B.; Huber, G. W. Plasmon-Enhanced Photoelectrochemical Water Splitting with Size-Controllable Gold Nanodot Arrays. *ACS Nano* **2014**, 8 (10), 10756−10765.

(42) Balachandran, U.; Eror, N. G. Raman Spectra of Titanium Dioxide. *J. Solid State Chem.* **1982**, 42 (3), 276−282.

(43) Ohsaka, T.; Izumi, F.; Fujiki, Y. Raman Spectrum of Anatase, TiO$_2$. *J. Raman Spectrosc.* **1978**, 7 (6), 321−324.

(44) Chih Lin, M.; Nien, L.-W.; Chen, C.-H.; Lee, C.-W.; Chen, M.-J. Surface Enhanced Raman Scattering and Localized Surface Plasmon Resonance of Nanoscale Ultrathin Films Prepared by Atomic Layer Deposition. *Appl. Phys. Lett.* **2012**, 101 (2), No. 023112.

(45) Kashyap, K. K.; Choudhuri, B.; Chinnamuthu, P. Enhanced Optical and Electrical Properties of Metallic Surface Plasmon Sensitized TiO$_2$ Nanowires. *IEEE Trans. Nanotechnol.* **2020**, 19, 519−526.

(46) Stroyuk, O. L.; Dzhagan, V. M.; Kozytskiy, A. V.; Breslavskiy, A. Ya.; Kuchmiy, S. Ya.; Villabona, A.; Zahn, D. R. T. Nanocrystalline TiO2/Au Films: Photocatalytic Deposition of Gold Nanocrystals and Plasmonic Enhancement of Raman Scattering from Titania. *Mater. Sci. Semicond. Process.* **2015**, 37, 3−8.

(47) Virga, A.; Rivolo, P.; Frascella, F.; Angelini, A.; Descrovi, E.; Geobaldo, F.; Giorgis, F. Silver Nanoparticles on Porous Silicon: Approaching Single Molecule Detection in Resonant SERS Regime. *J. Phys. Chem. C* **2013**, 117 (39), 20139−20145.

(48) Coluccio, M. L.; Das, G.; Mecarini, F.; Gentile, F.; Pujia, A.; Bava, L.; Tallerico, R.; Candeloro, P.; Liberale, C.; De Angelis, F.; Di Fabrizio, E. Silver-Based Surface Enhanced Raman Scattering (SERS) Substrate Fabrication Using Nanolithography and Site Selective Electroless Deposition. *Microelectron. Eng.* **2009**, 86 (4−6), 1085−1088.

(49) Torrell, M.; Kabir, R.; Cunha, L.; Vasilevskiy, M. I.; Vaz, F.; Cavaleiro, A.; Alves, E.; Barradas, N. P. Tuning of the Surface Plasmon Resonance in TiO2/Au Thin Films Grown by Magnetron Sputtering: The Effect of Thermal Annealing. *J. Appl. Phys.* **2011**, 109 (7), No. 074310.

(50) Brognara, A.; Mohamad Ali Nasri, I. F.; Bricchi, B. R.; Li Bassi, A.; Gauchotte-Lindsay, C.; Ghidelli, M.; Lidgi-Guigui, N. Highly Sensitive Detection of Estradiol by a SERS Sensor Based on TiO$_2$ Covered with Gold Nanoparticles. *Beilstein J. Nanotechnol.* **2020**, 11, 1026−1035.